Vol. 338: 81–96, 2007 | MARINE ECOLOGY PROGRESS SERIES
Mar Ecol Prog Ser | Published May 24

# Modeling coupling between eelgrass *Zostera marina* and water flow

**Mohamed A. Abdelrhman**

**US Environmental Protection Agency, Office of Research and Development, National Health and Environmental Effects Research Laboratory, Atlantic Ecology Division, 27 Tarzwell Drive, Narragansett, Rhode Island 02882, USA**

ABSTRACT: Ecological effects caused by submerged aquatic vegetation not only depend on the plants and their morphology but also on the flow and transport patterns of dissolved and suspended constituents near the canopy. Canopy height is a major variable in any quantitative analysis of plant biomass and constituent transport in its vicinity. Height of eelgrass *Zostera marina* canopies changes due to bending of the blades under varying current regimes. In this paper, I mathematically modeled the coupling between eelgrass blade bending and water flow. Based on the balance of forces of drag, lift, friction, weight and buoyancy on a single blade, the model defined the bending of blades (i.e. height of canopy) and the flow response within and above the canopy. This coupling was tested using laboratory data and indicated that the model performed adequately. Both model results and laboratory data confirmed that the bending of blades, and hence canopy height, was very sensitive to current magnitude and directly influenced current profile. Identifying canopy height is a major factor in defining spatial distribution of grass biomass from optical or acoustic remote sensing devices. The model has direct implications for biological issues related to the plants themselves and to their associated organisms, such as the vertical distribution of photosynthesis within the canopy and the effect of current shear on recruitment of organisms on the blades. It can also be used to study how eelgrass canopies affect horizontal transport of constituents, such as dissolved oxygen, nutrients and organic carbon, and particulate material such as pollen, larvae, plankton and detritus.

KEY WORDS: Model · Coupling · Eelgrass · Current · Canopy height · Shear · Photosynthesis



## INTRODUCTION

The importance of submerged aquatic vegetation (SAV) in general and eelgrass in particular to the well-being of marine ecosystems has been established and presented in numerous publications. SAV canopies increase resistance to flow (Short & Short 1984, Granata et al. 2001), which attenuates currents and causes suspended material, detritus and larvae to settle into the canopy (Ward et al. 1984, Gacia et al. 1999, Koch 1999). Enhanced sedimentation provides a situation where more biological species can exist (Granata et al. 2001). Meanwhile, intermeshed plants deflect part of the flow and protect the sediment, larvae, and plant roots from being scoured (Fonseca et al. 1982). Also, SAV shelters juvenile finfish and shellfish as well as grazers of algae. By trapping sediments, SAV keeps the water clear, which in turn increases the transmission of light and allows the plants to grow. Similarly, eelgrass affects transport conditions in its vicinity (Abdelrhman 2003) by altering the exchange of water, which affects sedimentation, recycling of nutrients and recruitment of fauna (Kenworthy et al. 1980, Eckman 1987, Rybicki et al. 1997). Seagrass meadows may be regarded as net sinks of detritus in areas with low currents and as sources in areas with high currents (Fonseca et al. 1983, Koch 1999). In addition to these ecological implications, meadows of eelgrass are sensitive bioindicators of water quality because they need fairly clear water and moderately low nutrients to survive. Consequently, these canopies may degrade as agriculture and shoreline development increase the nitrogen

*Email: abdelrhman.mohamed@epa.gov

concentration in the water and thereby increase phytoplankton to levels that limit the light reaching the grass (Dennison et al. 1993, Short & Burdick 1996).

The well-being of eelgrass canopies is essential both to the plants and to their inhabitors (e.g. juvenile finfish, shellfish, grazers of algae, fauna etc., as mentioned above), thus it is essential to monitor eelgrass canopies in sensitive areas. Three techniques exist to do this (Sabol et al. 1997, 2002): manual sampling with divers; optical reflectance from airborne photography; and acoustic scattering using a boat-mounted transducer. While manual sampling provides the most accurate data using actual samples from a certain location at a specific time, it becomes cost ineffective and prohibitive when applied to large regions at various times during a season or throughout many years of study. Airborne photography can provide wide spatial coverage of this habitat only when water clarity is adequate and plants are within the detectable layer. This technique may not work at the deeper edge of the canopy. Neither of the above-mentioned techniques provides the height of the canopy nor the actual vertical distribution of biomass within the canopy. On the other hand, acoustic back-scattering can provide canopy height along transects, which can be useful in studying ecological processes that depend on height within the canopy, e.g. current velocity, shear stress, larva attachment to blades and self-shading. A complicating factor for remote sensing techniques is that the height of the canopy is directly related to the strength of the current. This relationship has to be understood for any quantitative analysis of biomass.

Field observations (e.g. Kenworthy et al. 1980, Sabol et al. 1997) and laboratory experiments (Foncesa et al. 1982, Fonseca & Fisher 1986, Fonseca & Kenworthy 1987) indicate that eelgrass bending angle continuously changes in response to current magnitude and direction. During periods of slack tidal currents, the gas-filled tissue (lacunae) in the blades produce enough buoyancy to keep the blades erect and perpendicular to the bottom. However, lateral current may counteract this tendency and deflect the blades in the direction of the current. Strong current may cause the blades to lie flat over the bottom. Fonseca et al. (1982) indicated that blades reached their maximum bending at currents of ~50 cm $s^{-1}$, a figure that depended somewhat on plant density. They also indicated that the edge of the meadow was the most dynamic, where high bending increased self-shading and where the slowing of currents increased the deposition of suspended particles. Bending of the blades, canopy height and edge effects are addressed in this paper.

Many researchers have studied how plants affect currents and vice versa, both in the field (Fonseca et al. 1983, Ackerman & Okubo 1993, Grizzel et al. 1996) and in the laboratory (Fonseca et al. 1982, Fonseca & Kenworthy 1987, Gambi et al. 1990, Nepf & Vivoni 2000, Ghisalberti & Nepf 2002). Modeling is an comparatively inexpensive way to predict some of the ecological implications under various scenarios of plant physiology and current regime. Few models, however, tackle flow in and above SAV. Schutten & Davey (2000) used regression analysis of laboratory measurements to predict the hydraulic drag forces on various kinds of plants. Verduin & Backhaus (2000) presented a 3-dimensional numerical model that described the interactions between flow and *Amphibiolis antarctica*. The model predicted velocity profiles, kinetic energy and drag forces in and above the canopy. Their canopy model, however, did not include buoyancy, inertia, and vertical motion of the plants; thus, it did not reflect the actual height of the canopy. Kutija & Hong (1996) presented a steady-state 1-dimensional numerical model for vertical direction, to study the additional resistance to flow provided by flexible reeds. This model addressed the height of the canopy, but it was not calibrated or verified and it did not include the interaction of plants with the flow. None of the above-mentioned models dealt with eelgrass, which is extremely flexible. Abdelrhman (2003) presented a simple analytical model that offered empirical solutions to describe the effect of eelgrass beds on flow within and above dense canopies. The model did not resolve the coupling between flow and plants. The average canopy height was kept constant and roughly equal to the mean height of blades (assumed erect). Although these assumptions were made to present a simple, first order solution for the effect of eelgrass, they are not always met in nature.

The main goal of this work was to present a more sophisticated and realistic mathematical model to resolve the flow-plant coupling for eelgrass to a fuller extent. The specific objectives were to: (1) model the effect of current on the bending angle of blades and on canopy height; (2) model the effect of deflected blades on water velocity within the canopy; (3) calibrate and test the model with existing data from laboratory experiments; (4) define the effect of coupling on the distribution of horizontal shear within the canopy; and (5) define the effect of blade bending on the distribution of shade, in contrast to light, within the canopy.

## METHODS

**Dynamics of eelgrass.** The mathematical model presented here offers a solution that can work for both steady and time-varying flow within and above dense eelgrass. Only the effects of the canopy on vertical distributions of velocity are presented here, because the

canopy is assumed to be wide and homogeneous; lateral diversion of flow around the canopy is assumed to be zero.

For convenience, I assumed that flow through eelgrass shoots can be divided into flow within the blade layer and flow within the sheath layer. Sheaths were assumed to be stiff (Gambi et al. 1990) and to thus maintain a vertical position; only blades would bend (Fig. 1a). Blades were assumed to exist as separate blades (Fig. 1b) with homogeneous physical characteristics (e.g. width, thickness, wet density etc.) but variable lengths. However, the methodology allows for variations along the same blade and among blades as described below. The main hydrodynamic forces on the blade are fluid drag, lift force, skin friction and buoyancy. Elasticity of the blade is assumed to be zero, i.e. the blade is totally flexible. Thus, I represented the blade by a series of *n*-elements linked together by joints from the top-most element to the bottom element near the bed (Fig. 1c). These joints act like hinges that transmit force and allow rotation in a vertical plane coinciding with the direction of the currents, but do not transmit any moments. Each element was assumed to be straight and subject to a set of forces that represent the segment weight and buoyancy, fluid drag and lift, and skin friction (Fig. 1d). I ignored the effect on these forces of bubbles or other organisms (e.g. epiphytes) that may exist on the blades. Forces on an element produce reactions at the assumed joints. These reactions are passed to adjacent elements. The forces proceed through the blade from the top-element down to the sea bottom and are balanced by the anchoring reaction between the roots and the bottom.

In the shallow environments that eelgrass usually inhabit, water velocity can be assumed horizontal. The vertical distribution of current velocity is assumed to be known upstream from the leading edge of the canopy. The model defines changes in both the canopy and the flow downstream from the canopy's leading edge. The following analysis presents a quantitative evaluation of the forces exerted by the current on a single element *i* in a blade and the bending of that element (Fig. 1d). I assumed that the blade acts as an immersed flat plate and applied theoretical principles of boundary layer flow around plates (Schlichting 1960) to define the various hydrodynamic parameters, forces and coefficients.

A list of all variables and parameters used is given in Table 1.

**Weight.** The force due to weight of the element in air can be defined from its volume and density:

$$F_{\text{Weight}} = \rho_p g V \quad (1)$$

where $\rho_p$ is the wet density of the plant, $g$ is gravitational acceleration (980 cm $s^{-2}$) and $V$ is the volume

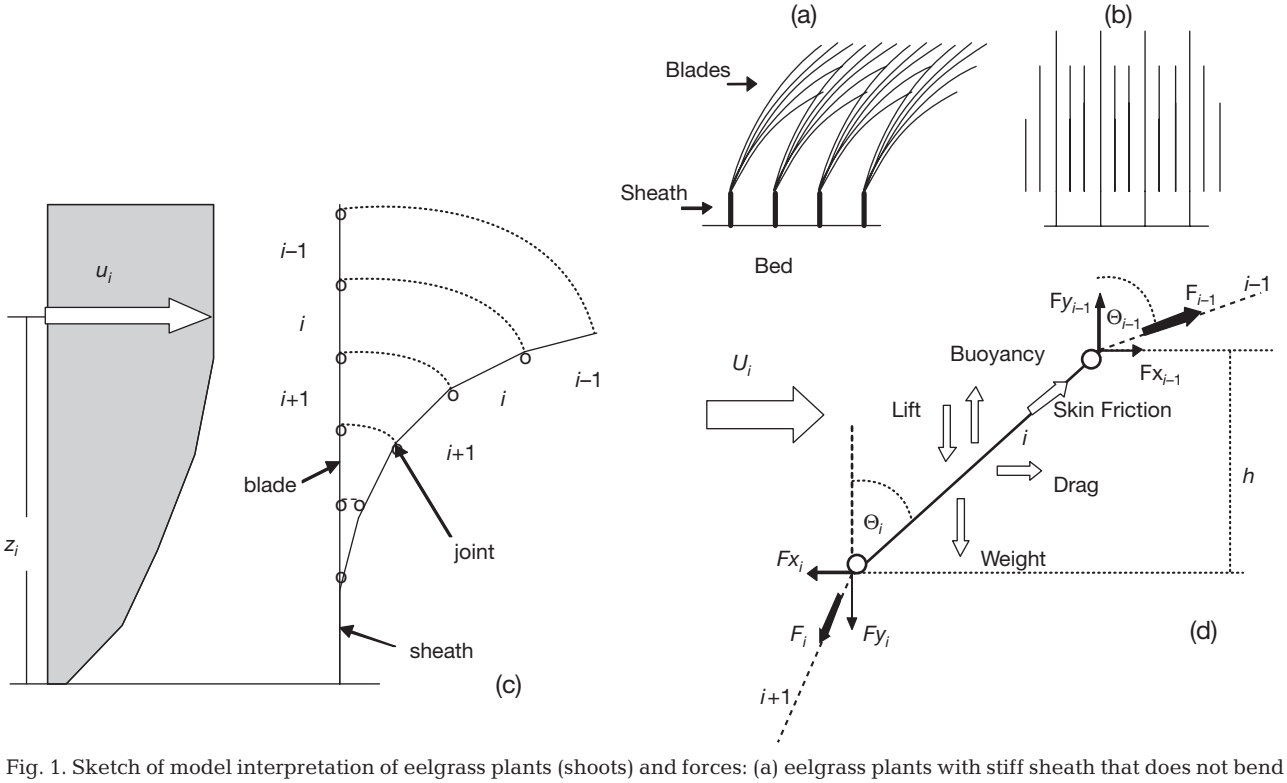


Fig. 1. Sketch of model interpretation of eelgrass plants (shoots) and forces: (a) eelgrass plants with stiff sheath that does not bend and flexible blades that bend; (b) plants as uniformly distributed sheaths with uniformly distributed separate blades; (c) effect of horizontal current $U$ on elements and joints of blade; (d) forces and reactions on a general element $i$

Table 1. Definitions of variables and parameters

| Quantity and dimension | Description |
|---|---|
| $A_l$ ($cm^2$) | Projected area of an element on a plane parallel to flow |
| $A_p$ ($cm^2$) | Projected area of an element on a plane perpendicular to flow |
| $A_s$ ($cm^2$) | Surface area of an element |
| $A$ ($cm^2$) | Vertical frontal area of deflected blades per unit volume |
| $C_d$ | Coefficient of drag |
| $C_f$ | Coefficient of friction |
| $C_l$ | Coefficient of lift |
| D | Density of blades |
| $F$ (dyne) | Force |
| $f$ | Normal distribution function |
| $G$ (cm $s^{-2}$) | Gravitational acceleration |
| $H$ (cm) | Total height of water column |
| $h$ (cm) | Height of deflected element or height of canopy |
| $i$ | Counter or subscript |
| $L$ (cm) | Mean length |
| $\ell$ (cm) | Element length |
| $N$ (blades $m^{-2}$) | Number of blades per unit horizontal area |
| $T$ (mm) | Mean thickness |
| $t$ (cm) | Element thickness |
| $u_h$ (cm $s^{-1}$) | Free-stream velocity at the top of canopy |
| $U$ or $u$ (cm $s^{-1}$) | Horizontal velocity |
| $u^*$ (cm $s^{-1}$) | Friction velocity |
| $V$ ($cm^3$) | Volume |
| $W$ (mm) | Mean width |
| $w$ (cm) | Element width |
| $x$ (cm) | Horizontal direction/distance in the direction of the flow |
| $\Delta$ (cm) | Minimum separation distance between blades |
| $y$ (cm) | Vertical direction/vertical location |
| $z$ (cm) | Height above the bed |
| $z_o$ (cm) | Height of bed roughness elements |
| $\Theta$ (degrees) | Deflection angle of an element from the vertical direction |
| $\Phi$ (degrees) | Angle of attack |
| $\rho_p$ (g $cm^{-3}$) | Density of plant |
| $\rho_w$ (g $cm^{-3}$) | Density of water |
| $\kappa$ | Von Karman's constant = 0.4 |
| $\alpha$ | Velocity attenuation coefficient |
| $\mu$ (cm) | Mean length of blade |
| $\sigma$ (cm) | Standard deviation of mean length of blade |
| $\lambda$ (cm) | Mixing length |

of the element: $V = w\ell t$, where $w$, $\ell$ and $t$ represent the element's width, length and thickness, respectively.

**Form drag.** As the fluid passes by each blade, it generates drag and lift forces. Two kinds of drag forces exist: form drag (also called pressure drag) in the direction of motion and skin friction drag in the direction of the element. Form drag results from the integration of dynamic fluid pressure on the blade in the direction of the flow (Schlichting 1960, p. 16; Vogel 1994, p. 164) and it can be expressed by:

$$F_{Drag} = \tfrac{1}{2} C_d \rho_w U^2 A_p \quad (2)$$

where $C_d$ is a drag coefficient, $\rho_w$ is mass density of water, $U$ is current speed, and $A_p$ is the projected area of the element on a plane perpendicular to the direction of flow. As the blade's inertia is always weaker in the direction perpendicular to its width, the blades are always assumed to align with their width facing the current. Assuming that the element will deflect in the flow direction at an angle $\Theta$ from the vertical direction, then $A_p = wh$, and $h = \ell \cos\Theta$. The angle $\Theta$ (i.e. orientation of the element) is the major unknown in this part of the analysis.

**Skin friction drag.** Roughness on the front and back surfaces of each blade generates the skin friction drag between the moving fluid and these stationary surfaces. This drag aligns in the direction of the element and can be expressed as:

$$F_{Friction} = \tfrac{1}{2} C_f \rho_w (U \sin\Theta)^2 A_s \quad (3)$$

where $C_f$ is the skin friction coefficient (assumed to be the same for the 2 sides of the blade), $A_s$ is the surface area of the element ($A_s = 2w\ell$), and $U \sin\Theta$ represents the component of current speed in the direction of the element (Schlichting 1960, p. 599; Vogel 1994, p. 301).

**Lift force.** As the fluid passes by the blade it produces a lift force in a direction perpendicular to the direction of velocity, which can be expressed by:

$$F_{Lift} = \tfrac{1}{2} C_l \rho_w U^2 A_l \quad (4)$$

where $A_l$ is the projected area of the element on a plane parallel to the direction of flow (i.e. $A_l = w\ell \sin\Theta$) and $C_l$ is the lift coefficient (Schlichting 1960, p. 16; Vogel 1994, p. 255). It is worth noting that if the angle between the direction of the horizontal flow and the direction of the element is oblique (i.e. $0 < \Theta < \pi/2$ ) the lift force will be downward; conversely, upward lift will occur when the flow approaches the element at acute angles (i.e. $\pi/2 < \Theta < \pi$ ). The latter case may appear when the element has negative buoyancy, e.g. leaves that are dead or infested with epiphytes or other organisms.

**Buoyancy.** When submerged, the gas-filled lacunae are subjected to an upward buoyancy force capable of keeping the blade almost erect in quiescent flow. This force can be expressed by:

$$F_{Buoyancy} = \rho_w g V \quad (5)$$

The common practice is to subtract Eq. (1) for weight from Eq. (5) for buoyancy, to obtain the net vertical force in the form:

$$F_{\text{Vertical}} = (\rho_w - \rho_p) g V \quad (6)$$

Positive values for this force indicate that the plant is lighter than water ($\rho_p < \rho_w$) and has positive buoyancy; the opposite is true for negative values.

**Balance of forces.** Fig. 1c,d presents the general layout of the elements, the vertical profile of the current and the forces on a general element *i*. Each element is assumed to have uniform physical characteristics and its center matches its centroid. All forces are assumed to act at the center of the element. The element should align in the same vertical plane of $U$ (Fig. 1c) at an angle $0 < \Theta < \pi$ (Fig. 1d). As mentioned above, the assumption that the blade is flexible (with zero elasticity) validated the use of elements and joints (Fig. 1d). As these joints do not transmit moment, the resultant of all forces and their reactions should align in the direction of the element.

The general algorithm solves for all elements. As the elements change their bending, they will change their vertical location above the bottom, hence, they will experience different local velocities. The algorithm takes into account both the bending angle of the element $\Theta_i$ and the local velocity $U_i$ at the center of the $i^{\text{th}}$ element.

At the top-most element ($i = 1$), the resultant of the drag, lift, skin friction and buoyancy forces causes the element to deflect and produces tensile force (pull) in the element. To calculate the magnitude and direction of the resultant force, all forces have to be decomposed into components in the horizontal $x$ and vertical $y$ directions. The summation of all moments at the lower joint is calculated and equated to zero in order to obtain the bending angle of the element measured from the vertical $y$ direction:

$$\tfrac{1}{2} C_d \rho_w U_1^2 w_1 \ell \frac{\ell}{2} \cos^2\Theta_1 + \tfrac{1}{2} C_l \rho_w U_1^2 w_1 \ell \frac{\ell}{2} \sin^2\Theta_1 - (\rho_w - \rho_p) g w_1 \ell t_1 \frac{\ell}{2} \sin\Theta_1 = 0 \quad (7)$$

Note that skin friction forces are not present because they act along the element and their moment at the lower joint is zero. I did not manipulate this equation further to match the form for a general element *i* as described below. The only unknown in Eq. (7) is $\Theta_1$ which is obtained iteratively.

The top-most element has only a lower joint as the upper end is free, so the reaction $F_1$ at this joint should fall in the direction of that element. For the element to be stable in its position, the summation of all components of forces in each of the $x$ and $y$ directions should equal zero:

$$Fx_1 + \tfrac{1}{2} C_d \rho_w U_1^2 w_1 \ell \cos\Theta_1 + C_f \rho_w U_1^2 w_1 \ell \sin^3\Theta_1 = 0 \quad (8)$$

$$Fy_1 - \tfrac{1}{2} C_l \rho_w U_1^2 w_1 \ell \sin\Theta_1 + (\rho_w - \rho_p) w_1 \ell t_1 g + C_f \rho_w U_1^2 w_1 \ell \sin^2\Theta_1 \cos\Theta_1 = 0 \quad (9)$$

where $Fx_1$ and $Fy_1$ are the horizontal and vertical components, respectively, of the reaction at the lower joint.

The reaction $F_1 = (Fx_1^2 + Fy_1^2)^{1/2}$ is obtained by substituting the value of $\Theta_1$ in Eqs. (8) & (9). A force equal in magnitude and opposite in direction to this reaction will transfer the effect of all forces on the top element ($i = 1$) through its lower joint to the succeeding element ($i = 2$). The same procedure is then applied to solve for the bending of this and, similarly, the succeeding element(s). For a general (intermediate) element $i$ the generalized forms of Eqs. (7), (8) & (9) are:

$$\tfrac{1}{2} C_d \rho_w U_i^2 w_i \ell \frac{\ell}{2} \cos^2\Theta_i + \tfrac{1}{2} C_l \rho_w U_i^2 w_i \ell \frac{\ell}{2} \sin^2\Theta_i - (\rho_w - \rho_p) g w_i \ell t_i \frac{\ell}{2} \sin\Theta_i + Fx_{i-1} \ell \cos\Theta_i - Fy_{i-1} \ell \sin\Theta_i = 0 \quad (10)$$

$$Fx_i + \tfrac{1}{2} C_d \rho_w U_i^2 w_i \ell \cos\Theta_i + C_f \rho_w U_i^2 w_i \ell \sin^3\Theta_i + Fx_{i-1} = 0 \quad (11)$$

$$Fy_i - \tfrac{1}{2} C_l \rho_w U_i^2 w_i \ell \sin\Theta_i + (\rho_w - \rho_p) w_i \ell t_i g + C_f \rho_w U_i^2 w_i \ell \sin^2\Theta_i \cos\Theta_i + Fy_{i-1} = 0 \quad (12)$$

where $Fx_i$ and $Fy_i$ are the horizontal and vertical components of the reaction at the lower joint $i$ respectively. Eq. (10) is solved iteratively for the value of $\Theta_i$ which is then substituted in Eqs. (11) & (12) to define the reaction force that will affect the next element ($i + 1$).

**Coupling between eelgrass and currents.** Coupling between eelgrass blades and the fluid appears in the direct impact of current speed on the bending of eelgrass blades and in return, the influence of eelgrass blades on modifying the current profile. This coupling will be more pronounced through eelgrass meadows where effects from many blades are integrated. First, the analysis for a single row of blades is presented, then this analysis is applied to successive rows.

The effect of a single row of blades on the velocity profile can be defined by solving the equations for conservation of mass and horizontal momentum across that row. As mentioned above, eelgrass will not only affect the velocity profile within the canopy, but also above it. I assumed a wide meadow where flow diversion to the sides of the canopy can be neglected. To conserve fluid mass, the flow will be enhanced in the overlying water column to compensate for its retardation within the grass layer. In the vertical sheet of fluid moving past a 100 cm segment of the row of blades with a velocity profile $U$, the fluid will experience resistance equivalent to the above-mentioned forces from the ensemble of blades within this length. For the hor-

izontal layer of fluid passing by each element of the blade, the equation for conservation of horizontal momentum can be written as:

$$\rho_w U_{ai}^2 A_{N_i} = \rho_w U_{bi}^2 A_{N_i} + Fx_i \quad (13)$$

where $U_{ai}$ and $U_{bi}$ are the approaching and departing velocities, respectively, at the vertical location of the centroid of element $i$; $A_{Ni}$ is the modified projected area on a vertical plane perpendicular to the direction of flow, which includes the effect of density of blades at the $i^{th}$ element ($A_{Ni} = 100\ell\cos\Theta_i N_i$, where $N_i$ is the density of blades, as described below). Subscripts a and b refer to velocities before and after the location of the blade, respectively. I assumed that the initial velocity profile, $U_{ai}$, upstream from the leading edge of the grass meadow is known from field observations, laboratory measurements or theoretical treatment, e.g. assuming a logarithmic profile. Eq. (13) and the initial velocity profile are used to calculate horizontal velocity past the first row of blades $U_{bi}$ which is then used as the approaching velocity for the following row of blades. This process can be continued until the terminal value of $U_{bi}$ reaches its theoretical estimate $u_z = u_h \exp[\alpha(z/h-1)]$, where $u_h$ is the velocity at the predicted top of the canopy (based on bending of the blades) and the attenuation coefficient $\alpha = h[c_d a/(2\lambda^2)]^{1/3}$ with $\lambda$ as the mixing length and $a$ the vertical frontal area of the deflected blades per unit volume. This theoretical solution can apply throughout the remainder of the meadow (Abdelrhman 2003).

The density of blades $N_i$ changes above the sheath layer due to variations in the length of blades. Assuming separate and erect blades (Fig. 1b), this parameter can be calculated from:

$$N_i = \frac{N \times D_i}{10^4} \quad (14)$$

where $N$ is the total number of blades per unit area ($m^2$) of the bottom, $D_i$ is the density of blades existing at the location of the $i^{th}$ element, and the factor $10^4$ converts units of area from $m^2$ to $cm^2$. $D_i$ is calculated for erect blades. Based on laboratory observations (see below), I assumed that as the blades bend under the effect of stronger currents their number (i.e. density) does not change. Thus, I assigned a specific $N_i$ to each element along the blade based on its $i$-value. The maximum density was always near the bottom (at the element just above the sheath) and lower densities took place further above the sheath (Fig. 1b). Elements close to the top of the grass layer had the lowest density and consequently the least $N_i$.

The initial density distribution (blades $m^{-2}$) can be obtained from statistical treatments of representative field samples and simple manipulations. I assumed that the length of the erect blades followed a normal distribution:

$$f(z) = \frac{1}{\sqrt{2\pi}\sigma} \exp\left(\frac{-(z-\mu)^2}{2\sigma^2}\right) \quad (15)$$

where $f(z)$ is the normal distribution function of the blade length above the sheath (note that $z$ and $i$ are interchangeable because $z$ equals the number of elements above the bottom times $\ell$), $\mu$ is the mean length of the blade and $\sigma$ is its standard deviation. I assigned densities within the range $\mu-2\sigma$ to $\mu+2\sigma$, which encompasses ~95% of all values of blade lengths. From the top of the grass layer downward, the respective cumulative distribution represents the percentage of blades that are equal to or longer than $z$:

$$D_z = 100\int_{\mu+2\sigma}^{z} f(z)\,dz; \qquad \mu+2\sigma \geq z \geq \mu-2\sigma \quad (16)$$

Density was set to zero above $z = \mu + 2\sigma$ and 100% below $z = \mu - 2\sigma$. Fig. 2 illustrates the good agreement between observed blade densities and those calculated from Eqs. (15) & (16).

A simplified version of the above equations can be used for the fluid layer within the sheaths. The layer's thickness equals the mean length of the sheaths. Sheaths can be assumed stiff (Gambi et al. 1990) and likely to maintain a vertical position. Thus, there is no coupling between sheaths and flow; only horizontal drag forces need be considered and Eq. (11) reduces to:

$$Fx_s + \tfrac{1}{2} C_d \rho_w U_s^2 W_s L_s = 0 \quad (17)$$

where subscript s refers to the sheath, with $W_s$ and $L_s$ representing its mean width and length, respectively.

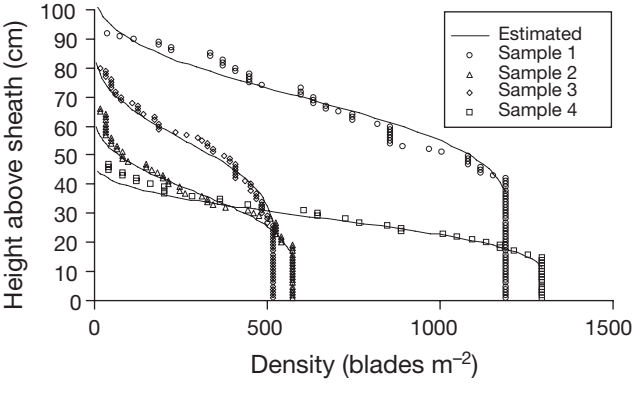


Fig. 2. Comparisons between estimated blade densities (blade $m^{-2}$, Eqs. 14 to 16) and measured values. The 4 field samples were obtained using 0.25 $m^2$ quadrats. Number and length of blades in Samples 1 to 4 were 1190, 574, 515, 1293 blades $m^{-2}$, with lengths 69 ± 6.4, 36 ± 10.4, 54 ± 8.1, 28 ± 6 cm, respectively

To calculate the change of velocity past each row of blades, Eq. (13) is modified to:

$$\rho_w U_{as}^2 A_{N_s} = \rho_w U_{bs}^2 A_{N_s} + F x_s \quad (18)$$

where $A_{Ns}$ is the modified projected area including the effect of sheath density, i.e. $A_{Ns} = 100\ L_s\ N_s$, with $N_s$ being the density of sheaths. Sheath effects are not considered in the following analysis of coupling, unless stated otherwise; see 'Discussion' for modeling of flow within sheath.

Conservation of mass requires that fluid mass before and after each row of blades be the same, i.e.

$$\int_H \rho_w U_a \, dz = \int_H \rho_w U_b \, dz \quad (19)$$

where $H$ is total water depth. The difference between $U_a$ and $U_b$ within the grass layer must be compensated for in the remainder of the water column above the canopy. Verduin & Backhaus (2000) indicated that the canopy can extend its influence to 1 m above the seabed, but further field observations are required to verify this statement. For simplicity and as a first order approximation, I assumed that this difference would be distributed uniformly throughout the overlying water column. Abdelrhman (2003) presented a rigorous theoretical solution that can apply to the flow above the canopy.

In summary, the spatial resolution of the model in the direction of the flow equals the minimum distance between the erect blades, Δ—at maximum blade density just above the sheath. In the vertical direction, the resolution is $\ell \cos\Theta_i$, which varies depending on the bending angle of the element. Thus, fluid flow and momentum are solved within an incremental volume defined as $100\Delta\ell\cos\Theta_i$ cm$^3$. Blade density within each incremental volume is given by Eq. (14).

**Model coefficients and parameters.** The characteristic length of flow (a length dimension that controls the flow) within emergent vegetation is usually taken as the stem diameter (Nepf et al. 1997, Nepf 1999). In eelgrass canopies this length will be the blade width. The Reynolds number for this width can be given by $R = uw\rho/\mu$, where ρ and μ represent water density and dynamic viscosity. Using typical values for flow and eelgrass ($U$ = 30 cm s$^{-1}$, $w$ = 0.5 cm, ρ = 1.027 g cm$^{-3}$, and μ = 0.014 g cm$^{-1}$ s$^{-1}$ at 10°C temperature and 35‰ salinity), R is $1.1 \times 10^3$, which indicates turbulent flow between the blades, with perhaps wakes and vortex shedding behind the blades (Nepf et al. 1997). I used existing empirical formulations (Schlichting 1968, p. 599) to calculate the skin friction coefficient. Assuming that the blades were smooth, the estimated skin friction coefficient was $C_f = 0.074\ R^{-1/5} \sim 0.02$. The lift coefficient $C_l$ varies with the angle of attack, i.e. the angle ϕ between the element and the approaching flow. It varies linearly from approximately −0.8 to 0.8 as ϕ changes from −15° to 15°. Beyond this range (i.e. |ϕ| > 15°) values of $C_l$ change non-linearly and drop sharply as ϕ reaches the stall angle, the same as for airfoils in aerodynamics. Thus, lift will be neglected when |ϕ| > 15°. The drag coefficient for a flat plate inclined to the flow changes linearly from ~0 to 0.2 for 0 < ϕ < 15°. I assumed that this linear variation will continue up to ϕ = 90° as $C_d$ becomes 1.2—a value consistent with literature estimates based on the aspect ratio of eelgrass (width/thickness~10) when R ~ 1000.

When several blades exist, sheltering effects can take place and may cause reduction in the drag force (Raupach & Thom 1981). For terrestrial canopies, a typical shelter factor (force on a single element/force on a group of elements) was estimated to be 3 to 4 (Thom 1971 for bean crop; Stewart & Thom 1973 for pine forests). Seginer et al. (1976) found a similar shelter factor (~3) from wind-tunnel experiments on cylindrical rods. All these values resulted from roughness elements that are erect and stiff, which produced well-developed wakes with clear shelter areas and shelter volumes behind them (Raupach 1992). In the case of the flexible non-erect eelgrass blades with various lengths, this factor is expected to be smaller because the resulting wakes, shelter areas and shelter volumes would be distorted. Unfortunately, similar estimates were not found for lift and skin friction forces. Until further research addresses this issue for marine canopies, I assumed that sheltering effects within eelgrass blades would reduce the above-mentioned coefficients for drag, lift and skin friction by a factor of 2.

The model requires information about grass morphology, including blade length, width, thickness, average number of blades per shoot and sheath length and width. This information has to be obtained from field samples. I collected field data in the vicinity of Rose Island in Narragansett Bay, Rhode Island (Abdelrhman 2003). I analyzed groups of 10 blades with lengths 30, 40, 50 & 60 cm and related blade parameters to its length. I also measured sheath length and width for a random sample of 130 shoots. The following regression forms (see Fig. 3) were derived from these data and were included in the model to provide first order estimates of plant dimensions in cm:

$$W_b = 0.0232 L_b + 3.3323; \quad r^2 = 0.8336 \quad (20)$$

$$T_b = 0.0028 L_b + 0.0636; \quad r^2 = 0.9848 \quad (21)$$

$$L_s = 0.1768 L_b + 5.2396; \quad r^2 = 0.5222 \quad (22)$$

$$W_s = 0.1923 L_s + 1.8117; \quad r^2 = 0.5545 \quad (23)$$

where $L_b$, $W_b$, $T_b$ represent mean length, width and thickness of the blades respectively, while $L_s$ and $W_s$

are sheath length and width respectively. In these regression equations, width and thickness are in mm and length is in cm. The model automatically converts $T$ and $W$ from mm to cm when they substitute for $t$ and $w$. Laboratory analysis indicated that the average wet density of blades, $\rho_p$, is 0.7 g cm$^{-3}$. The above information reduced model input parameters to: number of shoots per unit area; average number of blades per shoot; mean length of blades and its standard deviation. Knowing the initial velocity profile upstream from the leading edge of the canopy, the model generates the modified velocity profiles and the bending of the blades within the canopy.

## RESULTS

### Model coefficients

To check model coefficients, I used data collected from a laboratory flume (see below, 'Application of the model to laboratory data'). I recorded the bending of a single blade ($\ell_b$ = 45 cm, $w_b$ = 0.58 cm, $t_b$ = 0.022 cm) under gradually increasing currents (Fig. 4a) and used the balance of forces at various positions of the blade (Fig. 4b) to calculate drag, lift and friction coefficients. First, at velocity $V_4$, when the blade was almost horizontal, drag force was negligible and friction force was in the direction of the blade, i.e. horizontal. I used the balance between lift and buoyancy forces in the vertical direction to calculate the lift coefficient $C_l$ = 0.13. Second, at velocity $V_1$ with almost a vertical blade, I neglected friction force and used the balance of forces to calculate the drag coefficient $C_d$ = 0.7. To calculate the friction coefficient, all forces were considered with velocity $V_2$, which gave a value of $C_f$ = 0.07. I used $V_3$ as validation for all these coefficients. Three other replicates of single blades indicated similar qualitative behavior of the blades. All coefficients came within the same order of magnitude and values of the above mentioned coefficients were used in the model. It is worth mentioning that model coefficients depend not only on the age of the plant and the epiphytic growth on the blades but also on water properties (i.e. temperature and salinity), which directly affect its density and viscosity.

### Response of a single blade

I assumed that a boundary layer flow with a logarithmic velocity profile existed upstream from the leading edge of the grass canopy, i.e.

$$U_{ai} = \frac{u^*}{\kappa} \log_e\left(\frac{z_i + z_0}{z_0}\right) \quad (24)$$

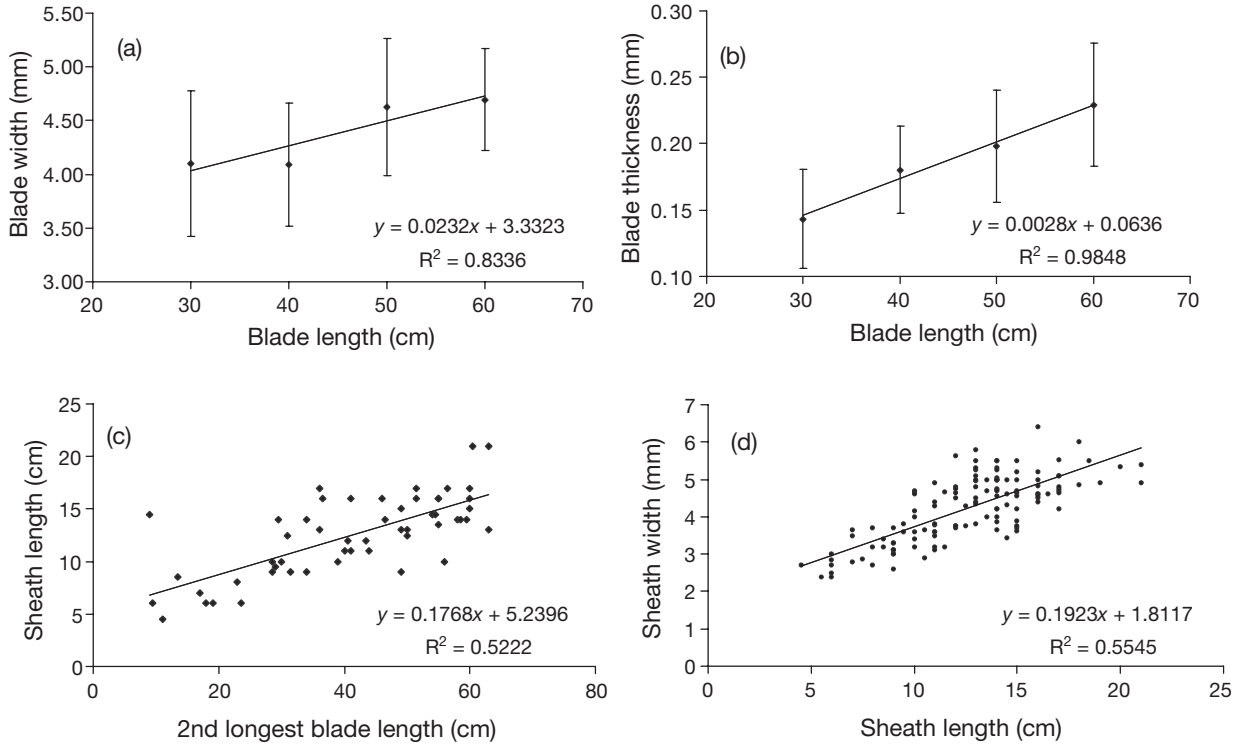


Fig. 3. Regression equations for eelgrass morphology derived from blade length: (a) blade width (mm); (b) blade thickness (mm); (c) sheath length (cm); (d) sheath width (mm). Error bars: ± 1 SD

where $u^*$ is the friction velocity, κ is von Karman's constant (κ = 0.4) and $z_o$ is bottom roughness, assumed to be 1 cm. Values of friction velocity 1 cm $s^{-1}$ and 3 cm $s^{-1}$ were applied to produce velocity distributions with maximum values of 10 cm $s^{-1}$ and 30 cm $s^{-1}$, respectively, at $z$ = 70 cm. Only the lower portion of the velocity profile, within the layer occupied by the deflected blade, was used. I tested the model with a hypothetical case with $\ell_b$ = 70 cm, $w_b$ = 0.5 cm, $t_b$ = 0.026 cm, $\rho_p$ = 0.7 g $cm^{-3}$, $\rho_w$ = 1.024 g $cm^{-3}$, $C_d$ = 0.7, $C_f$ =0.07, $C_l$ = 0.13 and $g$ = 980 cm $s^{-2}$. The blade was divided into 10 equal elements of 7 cm each.

Simulated deflections of the blade for $u^*$ = 1 cm $s^{-1}$ and 3 cm $s^{-1}$, respectively, are presented in Fig. 5a,b. As expected, higher velocities (Fig. 5b) caused more deflection of the blade. The height of the blade reduced from 60 cm to 27 cm when $u^*$ changed from 1 cm $s^{-1}$ to 3 cm $s^{-1}$. Although it is intuitive to expect that the smaller velocities of the logarithmic profile near the bottom would cause less bending of the lower elements than the top ones, this tendency was overcome by forces transmitted from the upper elements, which caused more bending to the lower elements (Figs. 5a,b).

I also tested velocity effects on blades with the upper half having density greater than that for water (e.g. a dead or infested part of the blade) and, thus, having negative buoyancy and causing that part of the blade to dangle down at weak currents (Fig. 5c, $u^*$ = 0.1 cm $s^{-1}$). As currents became stronger, lift forces pushed that part upward to align more in the direction of the currents (Fig. 5d,e for $u^*$ = 0.5 cm $s^{-1}$ and $u^*$ = 1 cm $s^{-1}$, respectively). Currents with $u^*$ = 3 cm $s^{-1}$ caused this part to approach its ultimate horizontal position (Fig. 5f). The peak height of the blade changed from 40 cm to 12 cm as $u^*$ changed from 0.1 cm $s^{-1}$ to 3 cm $s^{-1}$. Notice that the blade height in Fig. 5f is less than that in Fig. 5b due to the heavier, negatively buoyant upper half, which indicates that plants with negative buoyancy are expected to have more compact canopies.

### Velocity changes in a meadow

The effect of coupling is most pronounced at the edge of the meadow. Coupling is tested using an infinite meadow (1300 blades $m^{-2}$) of 38 cm long blades (σ = 0). The model calculated the values of $w_b$ = 0.42 cm (Eq. 20) and the minimum separation distance Δ = 2.78 cm. The shape of the originally logarithmic current profile (Eq. 24) was altered significantly into the meadow. Examples of this change are presented in Fig. 6 after the 1st, 100th and 200th rows of blades into the meadow (0, 2.8 and 5.6 m respectively). The effect was minimal after the first row, but after 2.8 m a flat S-shape appeared, with smaller velocities near the bottom and higher velocities at the top of the canopy. This S-shape became steeper after 5.6 m, as the shape became closer to that of the theoretical behavior presented in Abdelrhman (2003). Fig. 6b presents the shape and deflection of blades at these 3 locations. The maximum deflection appeared past the first row, which experienced maximum velocity values within the canopy. As distance into the meadow increased, the lower part of the blade was more erect, due to the retarded velocities, than the upper part, which experienced higher velocities. The effect of this coupling on the distribution of shear and shade are discussed later.

### Application of the model to laboratory data

I designed a recirculating flume (length = 7 m, width = 0.22 m, height and water depth = 0.6 m) to

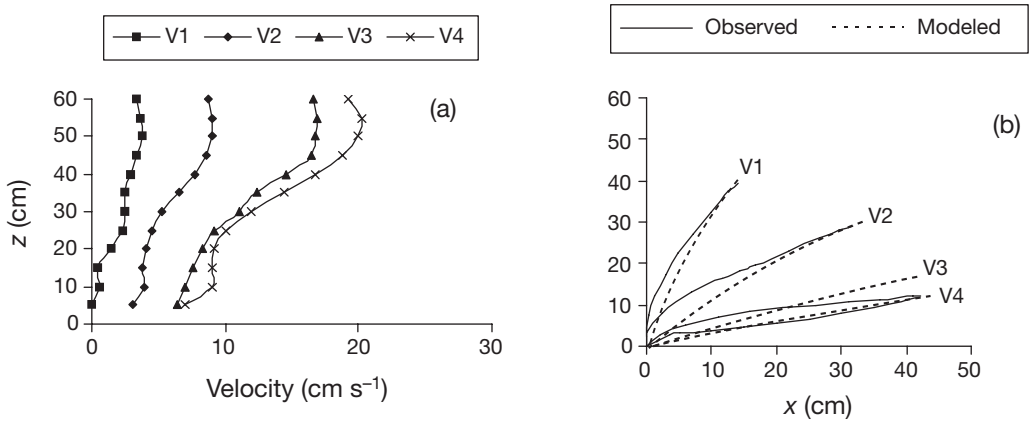


Fig. 4. Bending of a single blade ($\ell_b$ = 45 cm, $w_b$ = 0.58 cm, and $t_b$ = 0.022 cm) under gradually increasing currents: (a) velocity profiles V1 to V4 with approximate maximum values of 5, 10, 15 and 20 cm $s^{-1}$ respectively; (b) comparison between modeled and observed bending along single blade above sheath layer

study the dynamic behavior of eelgrass under the effect of currents (Fig. 7). A centrifugal pump circulated water at a maximum capacity of 600 gallons (= 2300 l) $min^{-1}$. Six velocity levels were obtained by controlling the flow using a ball valve on the delivery pipe and the throttle of the pump motor. I used a Marsh McBirney 2000 current meter (Marsh-McBirney 1990) to record velocity profiles at the center of the channel, at 5 cm increments throughout the water column, at a control location 0.5 m upstream from the leading edge of the canopy, and at 0.0, 0.5 and 1.0 m into the grass bed. The time constant for the current meter was set at 5 s and 5 replicates were recorded for each point-measurement of velocity. The average of the 5 replicates represented the velocity at that point. Shoots of eelgrass were attached at the most recent mature node on their rhizomes to a 23 × 100 cm bottom plate, using stoppers with 0.5 cm holes for rhizome, such that sheath and blades were freely exposed to the flowing water. The stoppers were arranged in rows every 3 cm along the plate; each had 7 stoppers, displaced inward or outward by 1.5 cm from the previous row to zigzag along the plate. When all holes were used, the maximum plant density was 1100 shoots $m^{-2}$. For each velocity level, this density was reduced successively by a factor of 2 to the lowest density of ~70 shoots $m^{-2}$, while keeping a spatially homogeneous distribution. Plants in length groups (based on the 2nd oldest blade) of 30, 40, 50 and 60 cm were tested separately and a population with a random mix of lengths was also tested. Looking through a glass window, a video camera and a

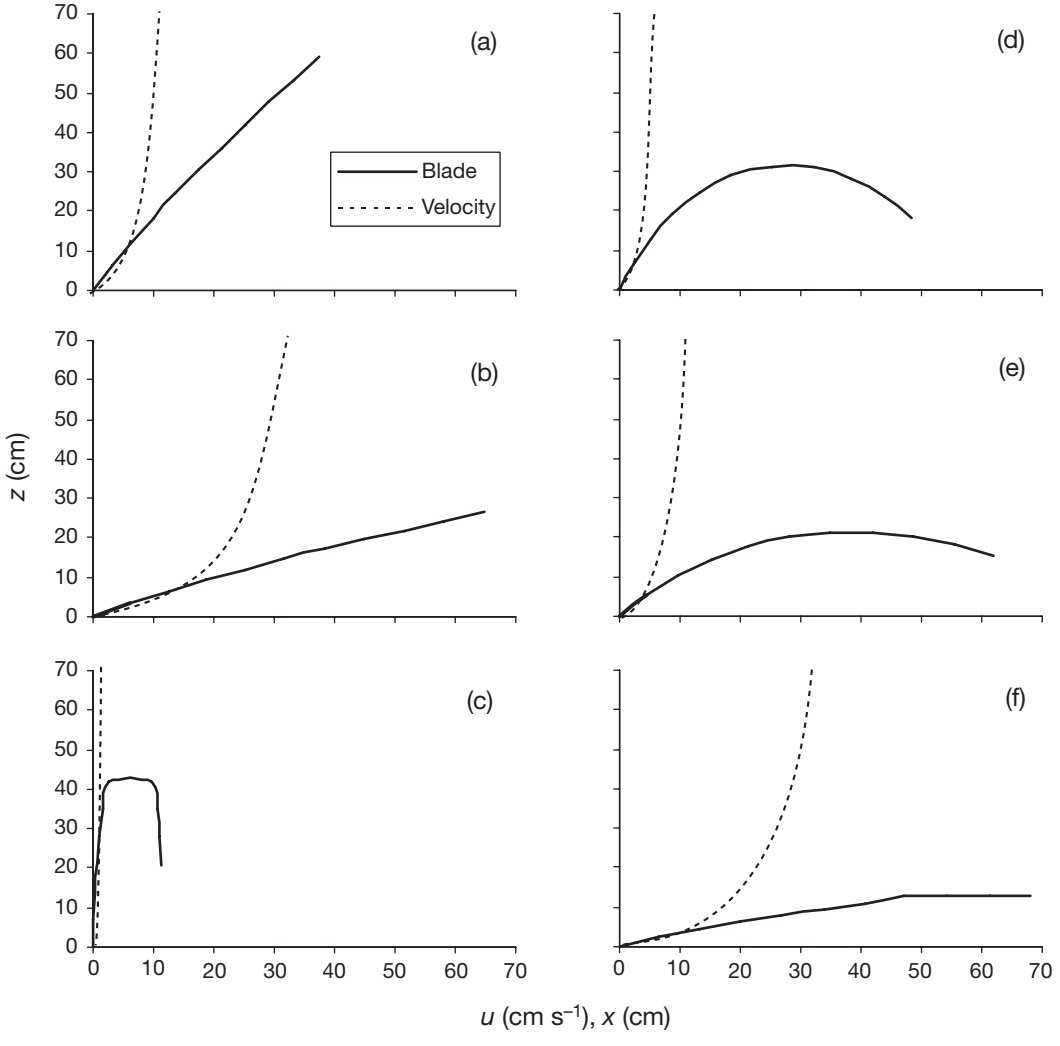


Fig. 5. Deflection of a blade ($\ell_b$ = 70 cm, $w_b$ = 0.5 cm, $t_b$ = 0.026 cm) due to logarithmic velocity profile in a 70 cm water depth: (a,b) velocity profile with $u^\star$ = 1 and 3 cm $s^{-1}$ respectively, on a healthy blade; (c–f) effect on a blade with negative buoyancy in upper half (e.g. epiphyte infested or dead) with $u^\star$ = 0.1, 0.5, 1 and 3 cm $s^{-1}$ respectively. In addition to velocity, horizontal axes represent horizontal distance $x$ in direction of flow

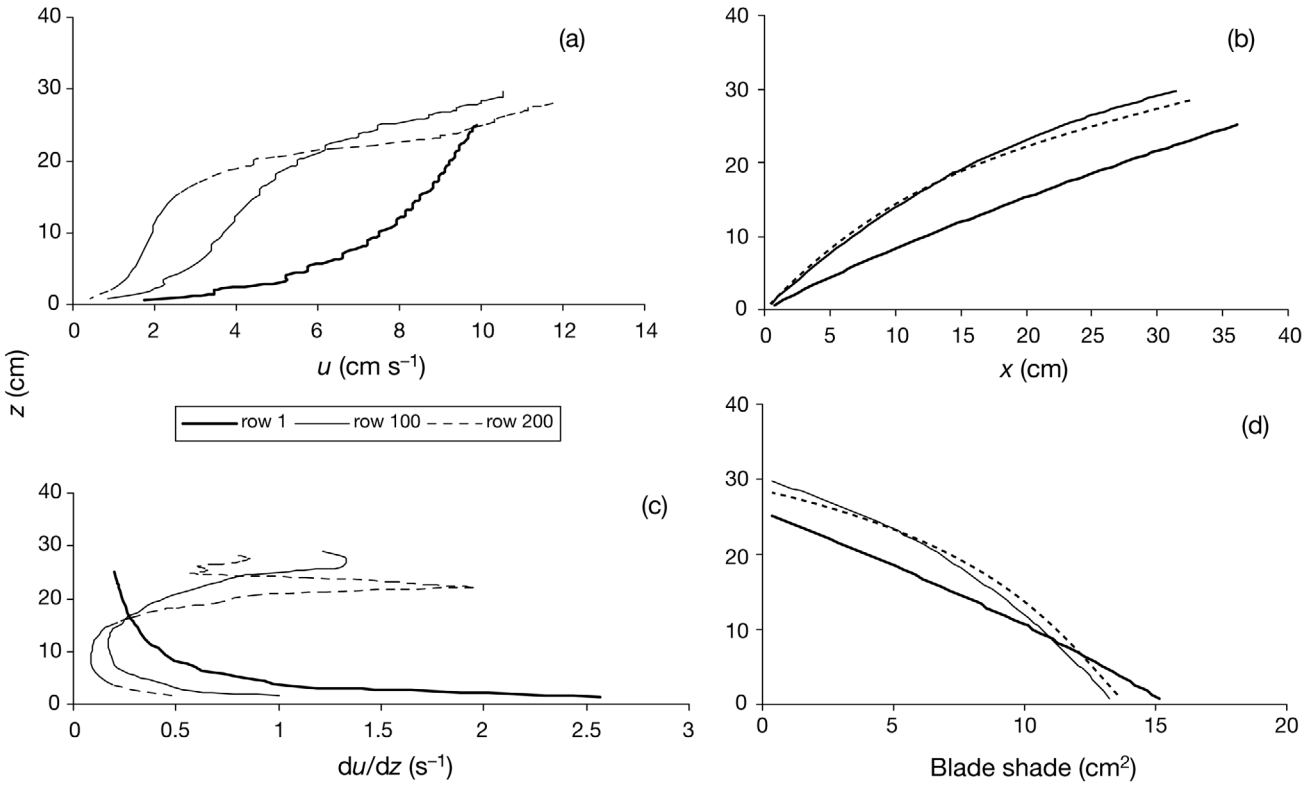


Fig. 6. Modeled effect of coupling between velocity and blades ($\ell_b$ = 38 ± 0, $w_b$ = 0.42 cm, $t_b$ = 0.02 cm) after 1, 100 and 200 rows: (a) change in vertical distribution of velocity; (b) shape and deflection of blade; (c) distribution of horizontal shear; (d) distribution of shade intensity

digital camera recorded plant movement. A grid with 5 × 5 cm divisions was drawn on the glass to define the bending of the blades. Examples of observed changes in eelgrass canopy under the effect of increased velocity are presented in Fig. 8.

I did not force the flume design to produce any specific velocity profile (e.g. logarithmic) because the model can be applied with any upstream velocity structure. In fact, as the length and density of the plants changed, they affected the recirculating flow and caused it to readjust to a new balance. Thus, I used the measured velocity profile at the control section as the base line for each scenario.

For model application, the above-mentioned calibration coefficients were used and water density was calculated as 1.024 g cm$^{-3}$, based on measured water temperature (20°C) and salinity (32‰). Examples of observed and modeled velocity profiles and blade bending (i.e. canopy height) are presented in Fig. 9 (1155 blades m$^{-2}$, $\ell_b$ = 25.4 ± 10.3 cm, $w_b$ = 0.5cm,

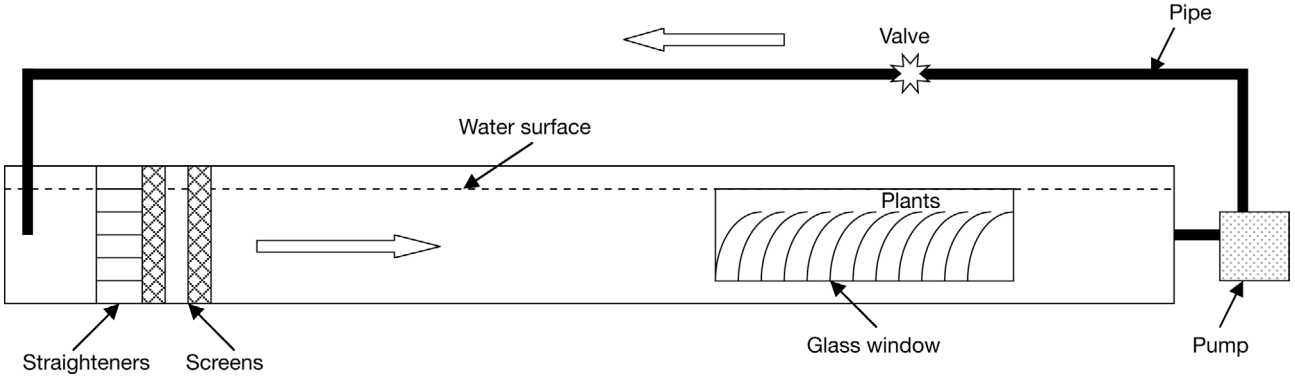


Fig. 7. Sketch of laboratory flume used to study eelgrass dynamics

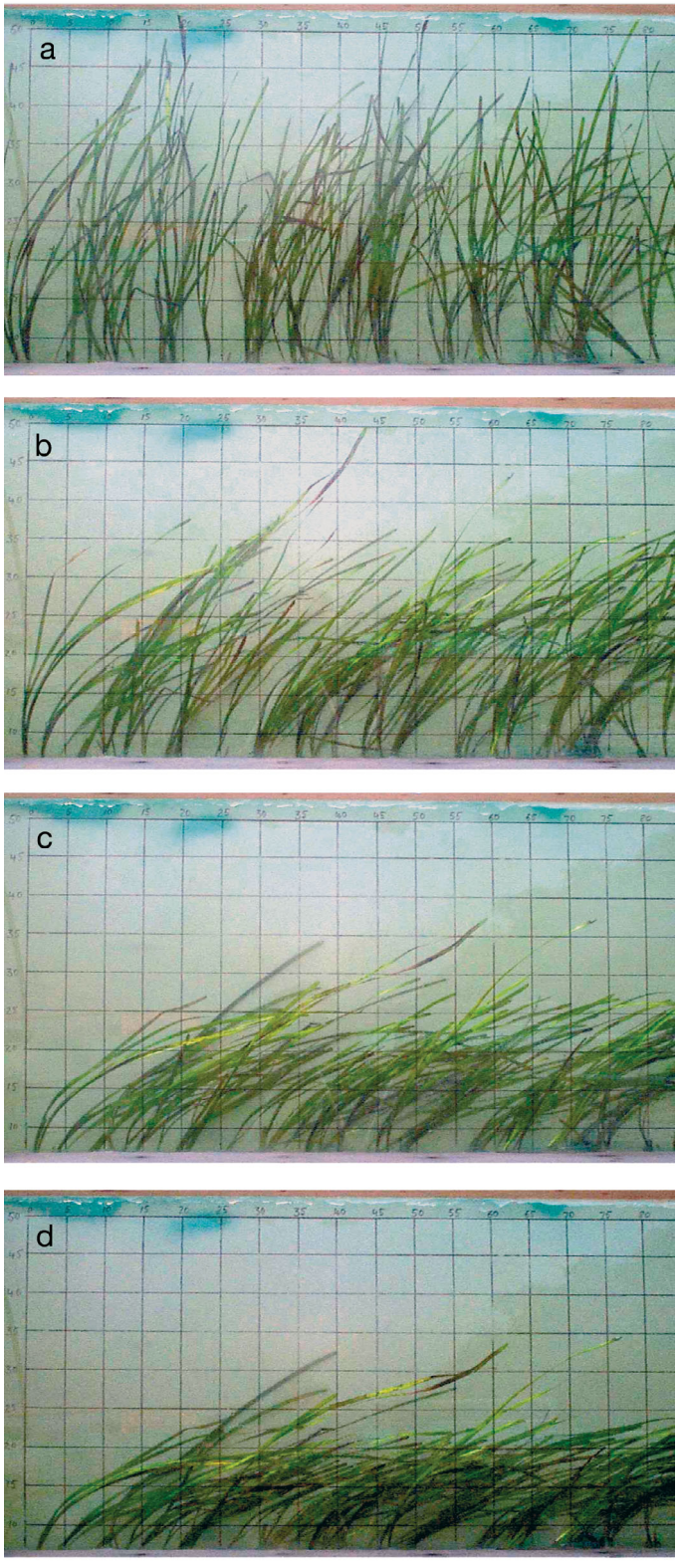


Fig. 8. Examples of the observed change in bending of ~40 cm long eelgrass blades in a meadow with 277 shoots $m^{-2}$ due to variation in current velocity: (a) zero velocity, (b) mean flow at 6 cm $s^{-1}$, (c) mean flow at 12 cm $s^{-1}$, (d) mean flow at 14 cm $s^{-1}$

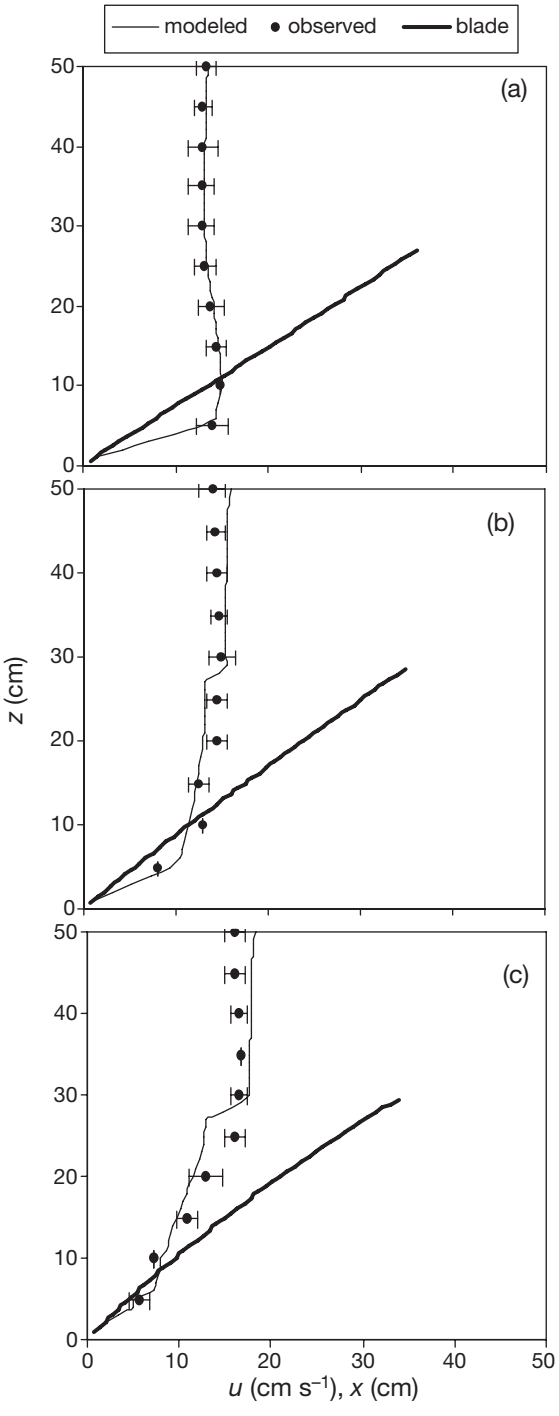


Fig. 9. Comparison between velocity profiles from flume observations (5 cm vertical resolution) and model results (1 cm vertical resolution) through a canopy with blade 25.4 ± 10.3 cm (length ± standard deviation) and density of 275 shoots $m^{-2}$ (i.e. 1115 blades $m^{-2}$): (a) at leading edge (after one row of blades), (b) at 50 cm from leading edge (at row 17), and (c) after 100 cm (at row 34). Each velocity observation is the average of 5 replicates; error bars: ± 2 SD. Bending of blade at each location indicates respective height of canopy. To show undistorted bending of blades, both vertical and horizontal resolution of axes are the same

$t_b$ = 0.035 cm). The model reproduced the height of the canopy (~25 cm) and the velocity structure within and above the canopy reasonably well.

## DISCUSSION

Based on the balance of forces on an eelgrass blade, I have presented a mathematical model to calculate the coupling between the velocity field and the bending of the blade. The model considers the vertical distribution of blade density (number of blades per unit horizontal area) and was calibrated, tested and validated with laboratory data, performing reasonably well in all cases.

The assumption of total flexibility of eelgrass blades can be revisited in future studies. Our laboratory observations indicate that buoyancy is the main factor restoring the deflected blades to a vertical posture. Elasticity is a second contributor and it is defined as the ability of the eelgrass blade (or part of it) to resist fluid drag forces. This effect is attributed to the flexibility of the blade. M. Fonseca & M. Koeh (pers. comm.) measured blade flexural stiffness ($EI$, where $E$ is Young's modulus of elasticity and $I$ is area moment of inertia, $wt^3/12$). They gave a value of $EI = 8 \times 10^{-8}$ Nm$^2$ for eelgrass blades; however, they stopped short of presenting the total deflection (i.e. bending) of the blades. Ghisalberti & Nepf (2002) indicated that the internal restoring moment in a blade is $M_I = EI\,\partial^2 z/\partial x^2$, where $z$ and $x$ are the Cartesian coordinates on the blade. They calculated the restoring force for artificial blades with $E = 3 \times 10^8$ Pa from this moment. The basic assumption in these studies is that the blade acts as a cantilever (i.e. column) subject to small deflection due to the lateral drag force. However, long eelgrass blades do not follow this description, rather they produce a whip-like motion (Ghisalberti & Nepf 2002). Niklas (1992, p. 153) presented discussions for the case of large deflections which may be combined with buoyancy effects in future studies to resolve the effect of blade flexibility on the restoring mechanism for eelgrass blades.

Other blade interactions that are not considered here may contribute to blade bending, e.g. physical interaction (i.e. touching) between blades resulting from local differences in movement of each element of the blade relative to elements of neighboring blades within its range of contact. However, our flume observations indicate that blade-blade interactions are very gentle and do not produce collision-like behavior, thus blade motion is controlled by the fluid around it rather than by other blades.

Although the volume occupied by the plants is not considered in the conservation of flow, it is included in momentum treatment in this model. The effective porosity may be estimated in cases with emergent fixed and stiff stems (e.g. Nepf et al. 1997, Nepf 1999), when the flow adjusts its speed and/or depth to conserve its mass flux. Nevertheless, observations for such well-defined settings showed inconsistencies throughout the depth (e.g. Nepf et al. 1997, their Fig. 5a). For submerged canopies such as eelgrass, this effect is even more ambiguous because some of the flow redirects above the canopy and does not have to proceed between the blades or stems. In addition, flexible blades with different lengths would add more complexity to this case. Nonetheless, using the maximum tested density of plants (1100 shoots, 4400 blades, $\ell_b$ = 25.3 cm, $w_b$ = 0.5 cm, $t_b$ = 0.035 cm), the ratio of blade volume to total volume within their layer is only 0.8% when blades are erect, and 2% when blades bend to $\theta \sim 70°$ and the layer reduces to only 10 cm thick. Porosity effects are not considered in contemporary modeling efforts for terrestrial or marine canopies. In the case of body force on stiff cylinders, Nepf & Vivoni (2000) neglected porosity effects. Such effects are also neglected here until dedicated laboratory experiments are conducted to quantify its impact — if any — on flow within eelgrass canopies.

The bending of the blades is important for remote sensing of the distribution of grass beds using airborne light or waterborne acoustic scattering techniques. These techniques can identify the spatial distribution of meadows but can rarely define biomass (mass of plants per unit of volume occupied by the plant or per unit area of the bed), which depends not only on spatial distribution but also on the height of the canopy. This difficulty is resolved by the model presented here, which can define the actual height of a canopy from the bending of blades observed in such field surveys. Thus, it is recommended that these surveys incorporate a methodology to estimate current profiles in the vicinity of grass beds, when biomass estimates are desired. These currents always change following tidal action and their spatial and temporal values can be estimated by hydrodynamic models. Another alternative is to have divers measure the *in situ* height of the canopy. Such measurements provide discrete local values at selected points and become cost-ineffective when repeated at various locations, during the changing tidal phases, or during seasonal variations of plant morphology. Alternatively, measuring plant dimensions from field samples may provide a distorted height of the canopy that does not reflect conditions during remote sensing surveys. In addition, exact estimates of this height have an inherent problem due to variability in blade lengths (Figs. 1a,b & 2), which dictates the use of a single representative length (e.g. mean), which neither reflects the actual length nor the actual *in situ* height of the canopy.

Together, this model and the model presented in Abdelrhman (2003) cover the entire grass meadow from the leading edge throughout the rest of the meadow. The model in Abdelrhman (2003) deals with the interior of the meadow assuming that the height of the canopy is known. This model calculates changes in canopy height from the leading edge to the interior of the meadow. These models may be adapted for use with multidimensional numerical models (e.g. Verduin & Backhaus 2000) capable of reproducing the required velocity field.

In addition to resolving the height of the canopy and its effect on flow, two important outcomes are obtained from the model presented here. First, the model resolves the change in horizontal shear within and past the leading edge of the meadow (e.g. Fig. 6c). For example, flow with an initially logarithmic velocity profile has maximum horizontal shear (d$u$/d$z$) near the bottom (see Fig. 6c, after 1 row of blades). This shear reduces to a minimal value in the overlying free stream flow. This shape changed after ~2.8 m into the meadow to a profile with 2 regions of high shear: one near the bottom and the other near the top of the canopy. The near bottom shear, however, was much less than that at the leading edge. Shear just below the top of the canopy increased to a maximum before it decreased to a smaller value, which may be attributed to both the effect of the reduced density of blades and the effect of the overlying free stream flow. Proceeding ~5.6 m into the canopy, the same shape existed, but with much reduced shear at the bottom and more enhanced shear near the top of the canopy. Shear near the top declined to values smaller than those at 2.8 m. As the flow proceeds further into the meadow the horizontal shear profile is expected to reach the shape presented in Abdelrhman (2003), with minimum value near the bottom and a maximum close to the top of the canopy.

The model addresses flow through the sheath layer. Although this layer is ~20% of shoot height (e.g. Fig. 3c), its proximity to boundary layer effects from the bed should not be underestimated. Gambi et al. (1990) measured flow profile within eelgrass including the sheath layer and indicated that higher velocities and turbulence existed within this layer. However, based on their sheath length (3.68 cm) and their sampling increment (1 to 2 cm), only a few velocity measurements could be sampled within the sheath layer, not enough to resolve velocity structure there. Methods to measure flow through the stems of stiff emergent plants (e.g. Nepf et al. 1997) at 1 cm increments may be used to study sheath flow in eelgrass. This case is more complex due to the overlying flow and flow within the layer of blades.

Simulated velocity and shear within sheath and blade layers ($\ell_b$ = 25.4 ± 10.3 cm, $w_b$ = 0.5 cm, $t_b$ = 0.035 cm, $\ell_s$ = 12.3 cm, $w_s$ = 0.52 cm) are illustrated in Fig. 10 for an originally logarithmic flow as it proceeds through the meadow at 50 cm and 100 cm from the leading edge in 50 cm of water. Fig. 10a presents details in the vertical distribution of the velocity profile. The model provides solutions within the 3 layers for sheath, blade, and overlying water in a stepwise fashion, which results in the sharp transitions (kinks) exhibited by the flow at boundaries between these layers (see also Figs. 9b,c). In reality, smoother transitions would exist due to plant morphology and motion as well as other flow factors including viscosity and turbulence. High velocity gradients (i.e. high shear) exist at the bed, at the top of the sheath and at the top of the canopy (Fig. 10b). The velocity gradient (shear) at the top of the canopy is the largest and that at the top of the sheath is negative. These gradients increase into the meadow, as velocities become more retarded at different rates within these layers. These shear zones may not be distinguishable for short shoots. Although this description of the change in shear is valid, the

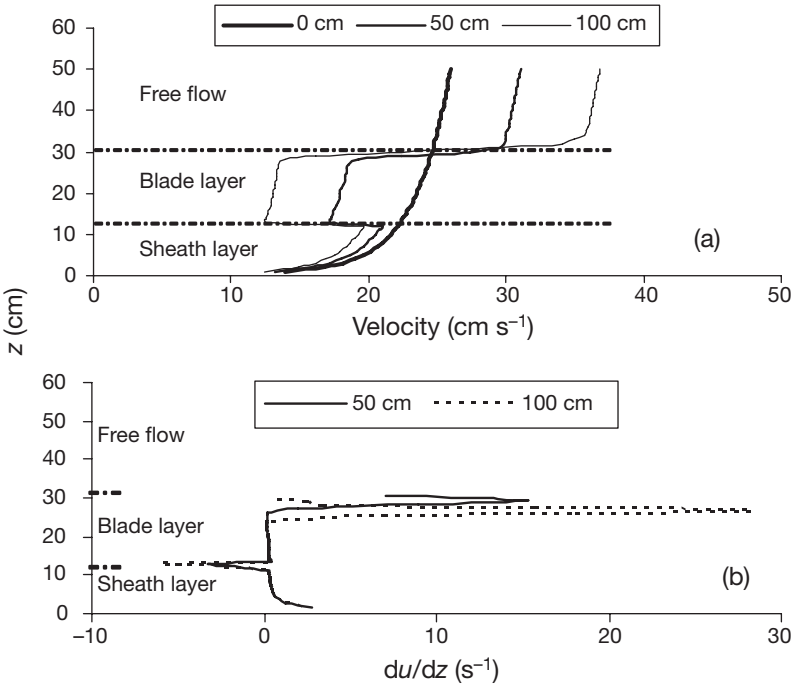


Fig. 10. Model results for velocity and shear of an initially logarithmic flow, including sheath layer: (a) velocity profile; (b) shear (d$u$/d$z$) within canopy, showing high values in vicinity of bed, top of sheath layer, and top of canopy

actual values are overestimates due to the above-mentioned kinks in the velocity profile. More measurements and analysis of flow within the sheath layer of eelgrass may be the subject of future studies.

Many ecological implications have a direct connection to the level of shear stress within a sea grass canopy: particulate resuspension and deposition, nutrient exchange, attachment of organisms (e.g. epiphytes, larvae) on the blades and pollination, among other things. Shear stress is produced from the relative motion between fluid layers, even when moving in the same direction, and indicates the level of turbulence in these layers. Fluid layers with high shear tend to counteract the settling velocity or hold suspended particles longer in the water column, detach or resuspend particles from adjacent surfaces (bed and leaves) and disperse or diffuse material more. Several authors (Gacia et al. 1999, Ward et al. 1984, Koch 1999) have indicated that SAV canopies attenuate currents and cause suspended material, detritus and larvae to settle into the canopy. The models presented here provide more information about the various horizontal and vertical zones within the canopy, where deposition or resuspension is more likely to take place. For example, with the high bed shear at the edge of canopy, only large suspended particles may settle, and proceeding into the canopy the lower bed shear is expected to winnow the settled particles into only the finer size classes. As mentioned in the introduction, sedimentation has many ecological repercussions in this habitat. Also, zones with low shear within the canopy (see Fig. 6c) are more suitable for recruitment of larvae (e.g. scallops). Based on model results, organisms may attach best near the top, in the vicinity of the immediate leading edge of the canopy, less well within the middle in the following area, and worst close to the lower zone further into the meadow. Different behavior is expected for nutrient exchange between the leaves and the water: high nutrient exchange is expected near the bottom at the leading edge, medium at the top and bottom of the following area, then high at the top further into the meadow.

The second important outcome from the model is the ability to define the amount of direct vertical shading from eelgrass blades and its distribution over the bed. Light is an important factor in the well-being of eelgrass and its inhabitants. The amount of incident light at the water surface diffuses in the water column and is attenuated as a result of water turbidity, such that only a fraction of it reaches the canopy in the form of direct and/or diffuse light. The existence of physical barriers (e.g. other blades) can significantly reduce the amount of light within the canopy. For example, considering direct light when the sun is perpendicular (at azimuth), each element of the blade will cast a shadow based on its bending angle, i.e. $\ell w \sin(\theta)$. The top element of the blade will cast a shadow relative to its area and the full shadow from a blade can be obtained by the cumulative addition of shadows cast by its elements from top to bottom. The cumulative value of shade is presented in Fig. 6d. As expected, shade increases from the top of canopy to its bottom. Also, blades that experience more bending (e.g. at the leading edge) produce more shade than those with less bending. Assuming no overlap and multiplying the cumulative amount of shade at each vertical location by the respective density of blades (e.g. Eqs. 14 & 16) produces the total shade per unit area at that height. For the above-mentioned test case with uniform density of plants (1300 blade $m^{-2}$, blade length = 38 cm, blade width = 0.42 cm, minimum separation $\Delta$ = 2.78cm), the shade from the whole community can be calculated by multiplying the shade from a single blade by the density of blades. The level within the canopy at which the community's shade reaches 1 $m^2$ defines the saturation level — below which the plants are totally shaded from incident light. The vertical distribution of the percentage of shade within the canopy is shown in Fig. 11. Overlap of the shadows from various blades produces saturation at a location deeper (from the top of the canopy) than when overlap is ignored: –15% overlap results in a ~22% increase in saturation depth (Fig. 11). Overlap effects can be investigated further in future research. It is worth mentioning that the effect of bending on light distribution within eelgrass canopies is just one aspect of a very complicated process that not only includes sun flecks, diffuse light, periods of exposure but also water quality effects on phytoplankton and epiphytic growth, and light attenuation.

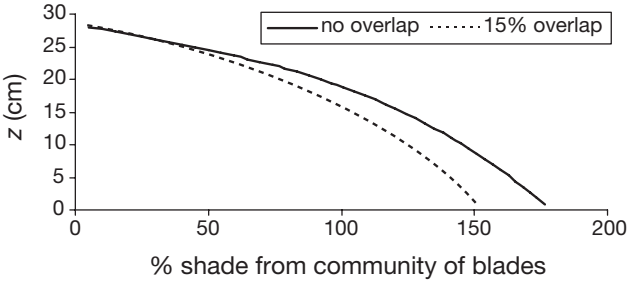


Fig. 11. Effect of blade deflection on shading (Fig. 6d) after 200 rows within a community of 1300 blades, 38 cm long with uniform vertical density of blades. Values >100% indicate full shading. Notice that height at full shading depends on blade deflection and overlap between shades, e.g. when canopy height was 28 cm, depth at saturation was 9.2 cm without overlap and 11.2 with 15% overlap

*Acknowledgements*: The author thanks D. Campbell, G. Thursby, G. Cicchetti (USEPA-AED) and 2 anonymous reviewers for their technical reviews, insight and constructive comments. I deeply appreciate the help of M. Abdalla with

hydro/aerodynamics derivations and K. Abdalla with morphology measurements and data input to spreadsheets. The research described in this article was funded by the US Environmental Protection Agency but has not been subject to Agency-level review and therefore does not necessarily reflect the views of the Agency, nor does mention of trade names or commercial products imply endorsement or recommendation. This manuscript is contribution no. AED-05-102 of USEPA Office Research and Development, National Health and Environmental Effects Research Laboratory, Atlantic Ecology Division.

## LITERATURE CITED

Abdelrhman MA (2003) Effect of eelgrass (*Zostera marina*) canopies on flow and transport. Mar Ecol Prog Ser 248: 67–83

Ackerman JD, Okubo A (1993) Reduced mixing in a marine macrophyte canopy. Funct Ecol 7(3):305–309

Dennison WC, Orth RI, Moore KA, Stevenson JC, Carter V, Kollar S, Bergstrom PW, Batiuk RA (1993) Assessing water quality with submerged aquatic vegetation. Bioscience 43: 86–94

Eckman JE (1987) The role of hydrodynamics in recruitment, growth, and survival of *Argopecten irradians* (L.) and *Anomia simplex* (D'Orbigny) within eelgrass meadows. J Exp Mar Biol Ecol 106:165–191

Fonseca MS, Fisher JS (1986) A comparison of canopy friction and sediment movement between 4 species of seagrass with reference to their ecology and restoration. Mar Ecol Prog Ser 29:15–22

Fonseca MS, Kenworthy WJ (1987) Effect of current on photosynthesis and distribution of seagrasses. Aquat Bot 27:59–78

Fonseca MS, Fisher JS, Zieman JC, Thayer GW (1982) Influence of the seagrass, *Zostera marina* L., on current flow. Estuar Coast Shelf Sci 15:351–364

Fonseca MS, Zieman JC, Thayer GW, Fisher JS (1983) The role of current velocity in structuring eelgrass (*Zostera marina*) meadows. Estuar Coast Shelf Sci 17:367–380

Gacia E, Granata TC, Duarte CM (1999) An approach to measurement of particle flux and sediment retention within seagrass (*Posidonia oceanica*) meadows. Aquat Bot 65:255–268

Gambi MC, Nowell ARM, Jumars PA (1990) Flume observations of flow dynamics in *Zostera marina* (eelgrass) beds. Mar Ecol Prog Ser 61:159–169

Ghisalberti M, Nepf HM (2002) Mixing layers and coherent structures in vegetated aquatic flows. J Geophys Res 107(C2):1–11

Granata TC, Serra T, Colomer J, Casamitijana X, Duarte CM, Gacia E (2001) Flow and particle distribution in a nearshore seagrass meadow before and after a storm. Mar Ecol Prog Ser 218:95–106

Grizzle RE, Short FT, Newell CR, Hoven H, Kindblom L (1996) Hydrodynamically induced synchronous waving of seagrass: 'monami' and its possible effects on larval mussel settlement. J Exp Mar Biol Ecol 206:165–177

Kenworthy WJ, Fonseca MS, Homziak J, Thayer GW (1980) Development of a transplanted seagrass (*Zostera marina L.*) meadow in Back Sound, Carteret County, North Carolina. In: Cole DP (ed) Proc 7th Annu Conf restoration and creation of wetlands, May 16–17, 1980. Hillsborough Community College, Tampa, FL, p 175–193

Koch EW (1999) Sediment resuspension in a shallow *Thalassia testudinum* banks ex König bed. Aquat Bot 65:269–280

Kutija V, Hong HTM (1996) A numerical model for assessing the additional resistance to flow introduced by flexible vegetation. J Hydraul Res 34:99–114

Marsh-McBirney (1990) Flo-Mate model 2000 portable water flowmeter instruction manual. Marsh-McBirney, Frederick, MD

Nepf HM (1999) Drag, turbulence, and diffusion in flow through emergent vegetation. Wat Resour Res 35(2): 479–489

Nepf HM, Vivoni ER (2000) Flow structure in depth-limited vegetated flow. J Geophys Res C 105:28547–28557

Nepf HM, Sulivan JA, Zavistoski RA (1997) A model for diffusion within emergent vegetation. Limnol Oceanogr 42(8):1735–1745

Niklas KJ (1992) Plant biomechanics. University of Chicago Press, Chicago, IL, 607p

Raupach MR (1992) Drag and drag partition on rough surfaces. Boundary-Layer Meteorol 60:375–395

Raupach MR, Thom, AS (1981) Turbulence in and above plant canopies. Annu Rev Fluid Mech 13:97–129

Rybicki NB, Jenter HL, Carter V, Baltzer RA, Turtora M (1997) Observations of tidal flux between a submersed aquatic plant and the adjacent channel in Potomac River near Washington, DC. Limnol Oceanogr 42(2):307–317

Sabol BM, McCarthy E, Rocha K (1997) Hydroacoustic basis for detection and characterization of eelgrass (*Zostera marina*). In: Proceedings of Fourth Conference on Remote Sensing for Marine and Coastal Environments, Orlando, Florida, 17–19 March, 1997. Environmental Research Institute of Michigan, Ann Arbor, Michigan p. I-679–693

Sabol BM, Melton Jr RE, Chamberlain R, Doering P, Haunert K (2002) Evaluation of a digital echo sounder system for detection of submersed aquatic vegetation. Estuaries 25(1):133–141

Schlichting H (1960) Boundary layer theory. McGraw-Hill, New York, NY

Schutten J, Davey AJ (2000) Predicting the hydraulic forces on submerged macrophytes from current velocity, biomass and morphology. Oecologia. 123:445–452

Seginer I, Mulhearn PJ, Bradely EF, Finnigan JJ (1976) Turbulent flow in a model plant canopy. Boundary-Layer Meteorol 10:423–453

Short FT, Burdick DM (1996) Quantifying eelgrass habitat loss in relation to housing development and nitrogen loading in Waquoit Bay, Massachusetts. Estuaries 19:730–739

Short FT, Short CA (1984) The seagrass filter: purification of coastal waters. In: Kennedy VS (ed) The estuary as a filter. Academic Press, London, p 395–413

Stewart JB, Thom AS (1973) Energy budgets in pine forest. QJR Meteorol Soc 99:154–170

Thom AS (1971) Momentum absorption by vegetation. QJR Meteorol Soc 97:414–428

Verduin JJ, Backhaus JO (2000) Dynamics of plant-flow interactions for the seagrass *Amphibolis antarctica*: field observations and model simulations. Estuar Coast Shelf Sci 50:185–204

Vogel S (1994) Life in moving fluids. The physical biology of flow, 2nd edn. Princeton University Press, Princeton, NJ

Ward LG, Kemp WM, Boynton WR (1984) The influence of waves and seagrass communities on suspended particulates in an estuarine embayment. Mar Geol 59:85–103

*Editorial responsibility: Kenneth Heck (Contributing Editor), Dauphin Island, Alabama, USA*

*Submitted: November 4, 2005; Accepted: September 27, 2006*
*Proofs received from author(s): April 23, 2007*